The role of Ca^{2+} and protein scaffolding in the formation of nature's water oxidizing complex

Anton P. Avramov[a], Hong J. Hwang[a], and Robert L. Burnap[a,1]

[a]Department of Microbiology and Molecular Genetics, Oklahoma State University, Stillwater, OK 74078

Edited by Pierre Joliot, Institut de Biologie Physico-Chimique, Paris, France, and approved September 21, 2020 (received for review June 6, 2020)

Photosynthetic O_2 evolution is catalyzed by the Mn_4CaO_5 cluster of the water oxidation complex of the photosystem II (PSII) complex. The photooxidative self-assembly of the Mn_4CaO_5 cluster, termed photoactivation, utilizes the same highly oxidizing species that drive the water oxidation in order to drive the incorporation of Mn^{2+} into the high-valence Mn_4CaO_5 cluster. This multistep process proceeds with low quantum efficiency, involves a molecular rearrangement between light-activated steps, and is prone to photoinactivation and misassembly. A sensitive polarographic technique was used to track the assembly process under flash illumination as a function of the constituent Mn^{2+} and Ca^{2+} ions in genetically engineered membranes of the cyanobacterium *Synechocystis* sp. PCC6803 to elucidate the action of Ca^{2+} and peripheral proteins. We show that the protein scaffolding organizing this process is allosterically modulated by the assembly protein Psb27, which together with Ca^{2+} stabilizes the intermediates of photoactivation, a feature especially evident at long intervals between photoactivating flashes. The results indicate three critical metal-binding sites: two Mn and one Ca, with occupation of the Ca site by Ca^{2+} critical for the suppression of photoinactivation. The long-observed competition between Mn^{2+} and Ca^{2+} occurs at the second Mn site, and its occupation by competing Ca^{2+} slows the rearrangement. The relatively low overall quantum efficiency of photoactivation is explained by the requirement of correct occupancy of these metal-binding sites coupled to a slow restructuring of the protein ligation environment, which are jointly necessary for the photooxidative trapping of the first stable assembly intermediate.

photosystem II | metalloprotein assembly | conformational fluctuation | oxygen evolution | water oxidation

Photosystem II (PSII) utilizes solar energy to catalyze one of the most important and most thermodynamically demanding reactions in nature: the oxidation of water into protons and molecular oxygen. The electrons extracted from the substrate water molecules are transferred through the redox-active cofactors of the photosynthetic electron transport chain eventually to reduce the electron acceptor $NADP^+$, thereby forming the primary reductant for the synthesis of biomass from CO_2 and other inorganic nutrients. Thus, the H_2O-oxidation reaction is the basis of oxygenic photosynthetic metabolism and the primary driver of biomass accumulation on the planet (1, 2) and represents a key chemical process for the development of carbon neutral energy technologies (3, 4). Natural H_2O oxidation is driven by light-induced charge separation within the PSII reaction center (RC), a 700-kDa membrane protein homodimer consisting of over 20 different subunits and ∼60 organic and inorganic cofactors (for reviews, see refs. 1, 2). The catalysis of H_2O oxidation is mediated by a metal cluster (Mn_4CaO_5) buried within the protein complex at the interface between intrinsic and extrinsic polypeptides toward the luminal surface of the photosynthetic membrane (5) (*SI Appendix*, Fig. S1). Photoexcitation of the multimeric chlorophyll (Chl) P_{680}, which functions as the primary photochemical electron donor, results in the primary charge separation on a picosecond timescale into the highly oxidizing radical cation P_{680}^+ and radical anion $Pheo^-$ (6). To minimize the backreaction or oxidation of Chl and/or neighboring proteins, the highly reactive P_{680}^+ is rereduced (20–250 ns) by the redox active tyrosine D1-Tyr161 (Y_z) of the D1 reaction center polypeptide located on the donor side proximal to P_{680}. Meanwhile, the energized electron is stabilized by transfer from $Pheo^-$ through quinone acceptors (Q_A and Q_B) and on through the remainder of the intersystem electron pathway leading to photosystem I. During the course of four consecutive charge separation events, the Mn cluster passes through a series of oxidant storage states (S-states) with the catalytic cycle balanced by removing four electrons from two bound water molecules with the release of O_2 and four protons.

The PSII complex is subject to incessant photodamage, and a remarkable feature is its ability to undergo self-repair. Photodamage primarily occurs within PSII, and much of the damage is localized in the D1 (PsbA) protein, which binds the main redox cofactors involved in photochemical charge separation. Efficient mechanisms have evolved to remove and replace damaged reaction center proteins and assemble them with their requisite cofactors (reviewed in ref. 7). A key step in both de novo synthesis and the repair synthesis of PSII is the assembly of the Mn_4CaO_5 core into the ligation environment of the PSII protein matrix (8–13). Referred to as photoactivation, the assembly of the Mn_4CaO_5 occurs through a series of photochemical reactions that involve the oxidation of Mn^{2+} ions using the same electron extraction pathway of the fully mature PSII (Fig. 1). Charge separation oxidizes Mn^{2+} ions to $Mn^{\geq 3+}$ as the oxo-bridged multinuclear metal center forms. The multistep process begins with the binding of a single Mn^{2+} ion (14), as its hydroxide (15) to a high-affinity site (HAS) involving the D1-Asp170 carboxylate

Significance

Unlike cofactor insertion into other metalloproteins, assembly of the photosynthetic water oxidation complex of photosystem II (PSII) in plants, algae, and cyanobacteria is a light-driven process that photooxidatively incorporates Mn^{2+} and Ca^{2+} ions into the protein matrix forming the catalytic Mn_4CaO_5 metal cluster. This self-assembly process is important both for de novo biogenesis and for the frequent repair of PSII due to its susceptibility to photodamage. While the basic kinetic scheme for this process was established nearly 50 y ago, the molecular details have remained enigmatic. Here we describe results on the role of inorganic and protein cofactors and integrate them with previous information to obtain an important upgrade in our understanding of this process.

Author contributions: A.P.A., H.J.H., and R.L.B. designed research; A.P.A. and H.J.H. performed research; A.P.A. and R.L.B. analyzed data; and A.P.A. and R.L.B. wrote the paper.

The authors declare no competing interest.

This article is a PNAS Direct Submission.

[1]To whom correspondence may be addressed. Email: rob.burnap@okstate.edu.

This article contains supporting information online at https://www.pnas.org/lookup/suppl/doi:10.1073/pnas.2011315117/-/DCSupplemental.

First published October 26, 2020.

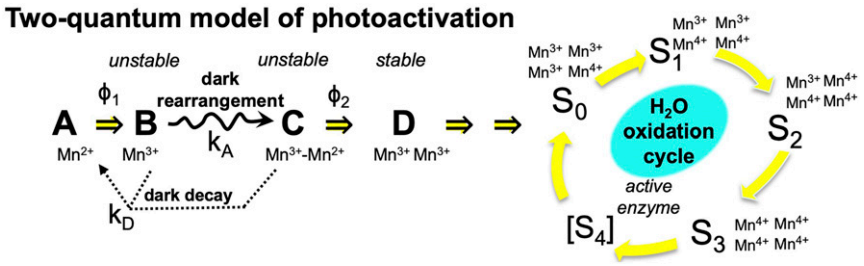

Fig. 1. Kinetic scheme of basic two-quantum mechanism of PSII photoactivation. Double arrows indicate light-activated processes with the quantum efficiencies Φ_1 and Φ_2 representing the first and second photooxidative events in the assembly sequence, k_A representing the dark rearrangement, and k_D representing the decay of intermediates. After the initial two Mn are photoligated, subsequent Mn appear to be added with high quantum efficiency.

moiety (16, 17). Additional Mn^{2+} ions are photooxidatively incorporated into the growing metal cluster via the oxo-bridges that are presumably derived from water ligands of the incoming metal ions. The quantum efficiency of photosynthetic H_2O oxidation in the fully functional PSII is greater than 90%. In contrast, the photoassembly of the metal cluster is remarkably inefficient with an overall quantum efficiency below 1%, despite the fact that photooxidative assembly uses the same charge separation cofactors, including the oxidized forms of the primary and secondary electron donors, P_{680} and Y_Z, respectively. To account for the low quantum efficiency and for a still unresolved light-independent "dark rearrangement" that must occur between two or more light-induced charges, a so-called "two-quantum model" (Fig. 1) was developed (8). Experimental support for this kinetic model is comprehensive (reviewed in refs. 7, 18), including, for example, direct evidence tracking the assembly process demonstrating a two-quantum requirement, and that part of the overall inefficiency is due to the competition between the slow and/or inefficient assembly steps and back-reactions of the charge-separated state (19). Nevertheless, evidence regarding the structure and chemistry of the intermediates and the nature of the dark rearrangement has remained scarce.

Calcium is a critical cofactor in the process of H_2O oxidation by PSII because it mediates the delivery of substrate water to a Mn coordination site for oxidation and dioxygen formation (20). While an early study suggested that Ca^{2+} is not required for photoassembly of the Mn cluster (21), this was later reevaluated (22), and there is now general agreement that Ca^{2+} is vital (11, 13, 22). Nevertheless, the mechanism of how Ca^{2+} facilitates the photoassembly remains obscure. Binding of Mn^{2+} to the HAS with simultaneous binding of Ca^{2+} to an adjacent binding site facilitates the formation of the [Mn^{2+}-(OH)-Ca^{2+}] complex by inducing deprotonation of a water ligand of Mn^{2+}. Calcium lowers the pK_a for water ligand, which is controlled by a nearby base B^- that serves as a primary proton acceptor with a pK_a dependent on Ca^{2+} bound to its effector site (23). The deprotonation of the intermediates and the tuning of pK_as facilitated by Cl^- binding is critical for assembly (24). The absence of Ca^{2+} during photoactivation leads to the formation of noncatalytic, multinuclear high-valence Mn species ("inappropriately bound Mn") that inactivates the PSII complex (22). At the same time, high concentrations of the Ca^{2+} cofactor diminishes the efficiency of photoactivation. These results indicate that Ca^{2+} and Mn^{2+} compete for each other's binding sites, leading to an optimality relationship in their relative concentrations during photoactivation (11–13).

Three extrinsic polypeptides, PsbO, PsbV, and PsbU, serve to enclose and stabilize the cyanobacterial water oxidation complex (WOC), whereas plants and certain eukaryotic algae possess PsbO, PsbQ, and PsbP (for review, see ref. 25). The extrinsic polypeptides prevent the reduction of the Mn cluster by exogenous reductants (26–28) and help retain the Ca^{2+} cofactor, which is otherwise prone to loss during the catalytic cycle (29, 30). However, by enclosing the WOC, accessibility of ions for the photoactivation of the Mn_4CaO_5 may be restricted. Indeed, the most efficient in vitro photoactivation procedures either explicitly or coincidentally involved the biochemical removal of the extrinsic proteins, and genetic deletion of the most evolutionarily conserved extrinsic protein, PsbO, increases the quantum efficiency of photoactivation (7). Proteomic analysis of highly intact cyanobacterial PSII revealed novel proteins, including a small protein designated Psb27, apparently associated with PSII subpopulations (31). Psb27 was identified as a lipoprotein associated with inactive PSII monomers that prevents binding of PSII extrinsic subunits (PsbO, PsbU, and PsbV) to the premature PSII (32), keeping the active site "open" and thereby maintaining a sufficient diffusion rate of Mn^{2+}, Ca^{2+}, and Cl^- ions, thus acting as a molecular chaperone for successful photoactivation (33), and does so through a specific interaction with the E-loop of CP43, which is a luminal domain of PSII that directly interacts with the Mn_4CaO_5. Overall, Psb27 appears to be strictly associated with organisms possessing PSII and is important for its assembly (34–37), yet its precise role in facilitating assembly remains to be resolved. The application of in vitro photoactivation procedures using genetically tractable cyanobacteria has not been described, and here we describe such a system and use it for the analysis of the roles that Ca^{2+} and Psb27 play in the assembly of the Mn_4CaO_5.

Results

Mn^{2+} and Ca^{2+} Competition during Photoassembly Leads to Decreased Quantum Efficiency and Yield during Photoactivation of Cyanobacterial Membranes. We developed a procedure for isolating Mn-depleted thylakoid membranes from *Synechocystis* sp. PCC6803 (hereafter, *Synechocystis*), enabling control of the photoactivation conditions, such as pH and ion composition, as well as permitting facile genetic modification of the constituent proteins. Importantly, the membranes retain the native electron acceptor system, so that artificial electron acceptors are not necessary as in previous in vitro experimental systems. Mn-depleted membranes produced by hydroxylamine (HA) extraction showed substantial restoration of photosynthetic activity (40%) (*SI Appendix*, Fig. S2*A* and Table S1), consistent with published yields in plant preparations (see ref. 12 for quantitative analysis), and, most importantly, display similar kinetic features of photoactivation compared to plant membrane preparations and to in vivo photoactivation experiments in *Synechocystis* (*SI Appendix*, Fig. S3). We focused on the role of Ca^{2+} in photoactivation and how the extrinsic proteins modulate the demand for both Mn^{2+} and Ca^{2+}. As shown previously, photoactivation requires presence of both Mn^{2+} and Ca^{2+} cations for the assembly of PSII, and postaddition of Ca^{2+} after illumination only resulted in a very small increase in the yield of active PSII (*SI Appendix*, Fig. S2*B*). Postaddition of Sr^{2+} or Mg^{2+} cations in the dark did not result in a significant yield of photoactivation. Thus,

our results concur with the general conclusion that Ca^{2+} is absolutely required for the assembly process (11, 13, 22).

In plant preparations, optimal photoactivation, both in vitro (12, 13, 38) and *in organello* (11), requires an optimal Ca^{2+}/Mn^{2+} ratio characterized by an excess of Ca^{2+} relative to Mn^{2+}, which reflects a competition between the ions for their respective binding sites (12). To establish whether similar kinetic features operate in cyanobacteria, the Ca^{2+} concentration dependence of photoactivation was performed at two fixed Mn^{2+} concentrations, 250 or 500 μM (Fig. 2 *A* and *B*). These concentrations of Mn^{2+} should saturate its binding to the HAS (13), but should still allow observation of the predicted competition between the two cations observed in plant preparations (11–13). A small level of photoactivation can be seen in the absence of added Ca^{2+} ions, which could be explained by trace amounts of residual Mn^{2+} and Ca^{2+} ions remaining in the extracted thylakoid preparation, since the level of this activity could be minimized, but never completely eliminated, by extensive washing of membranes using Chelex-treated buffer. For all of the samples containing 250 μM Mn^{2+} in photoactivation buffer, the maximum yield of photoactivation was observed at 600–700 flashes, with the half-maximal yield at occurring with ~150–200 flashes (Fig. 2*A*). In terms of maximal yield and quantum efficiency of photoactivation, the optimum Ca^{2+} concentration for photoactivation at 250 μM Mn^{2+} occurs at 10 mM, corresponding to Ca^{2+}/Mn^{2+} ratio of 40:1. The decrease in O_2 evolution at lower Ca^{2+} concentrations is likely caused by the competitive binding of Mn^{2+} to the Ca^{2+} binding site. In the context of earlier findings, this would prevent the formation of a bridged species [Mn^{3+}-(OH)-Ca^{2+}] that is proposed to be a crucial intermediate during the assembly (23), and perhaps leading to the formation of inappropriately bound high-valence, multinuclear Mn deposits (22). To better understand the role of ion competition and test the hypothesis that Mn^{2+} binding at the Ca^{2+} site leads to photoinactivation of PSII during photoassembly, we carried out the same experiment, but doubling Mn^{2+} concentration to 500 μM (Fig. 2*B*). For the optimum photoactivation at 500 μM Mn^{2+} the requirement for Ca^{2+} increased two-fold. Interestingly, samples containing 20 and 40 mM of Ca^{2+} in photoactivation buffer started to show signs of photoinactivation observed earlier at low Ca^{2+} concentration at 250 μM Mn^{2+}. From these results we can conclude that an excess of Mn^{2+} ions leads to the decreased yield of PSII photoactivation due to photoinactivation, while excess of Ca^{2+} ions does not have such effect.

To analyze the role of Ca^{2+} concentration on quantum efficiency of photoactivation and photoinactivation as a function of flash number and to better understand inhibitory effect of low Ca^{2+} to Mn^{2+} ratios, data described in Fig. 2 was fit to a double exponential equation:

$$[A]_n = [\mathrm{A}]_0 \cdot \left(1 - e^{\Phi_{PA} \cdot n}\right) \cdot \left(e^{-\Phi_{PI} \cdot n}\right) \qquad [1]$$

The equation accounts for the progressively smaller pool of apocenters during the flash sequence as more centers become photoactivated (10), combined with a term that represents the loss of centers due to photoinactivation processes (12). Here, $[A]_n$ represents the yield of active centers on the nth flash, whereas $[A]_0$ is the concentration of apo-PSII centers prior to the photoactivation, Φ_{PA}, which represents the overall efficiency of the multiphoton assembly process. The photoinactivation

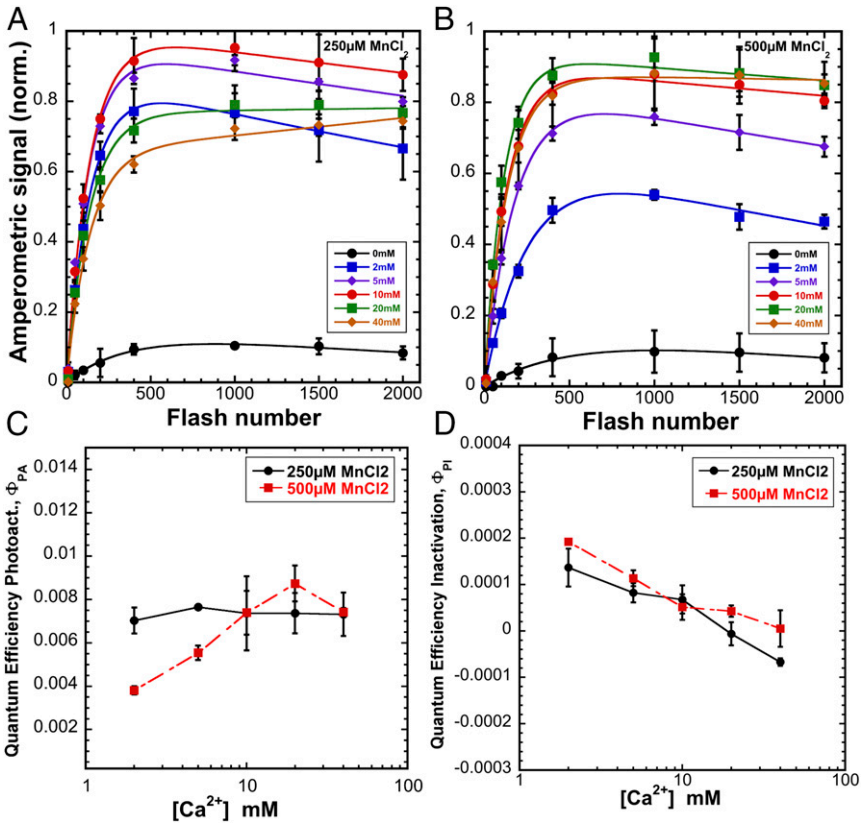

Fig. 2. Calcium dependence of photoactivation under sequence of single turnover flashes at 2 Hz (500-ms flash interval) of HA-extracted thylakoid membranes from WT control at 0 (black circle), 2 (blue square), 5 (purple diamond), 10 (red circle), 20 (green square), and 40 (orange diamond) mM of $CaCl_2$ combined with 250 μM (*A*) or 500 μM $MnCl_2$ (*B*). (*C*) Overall quantum efficiency of photoactivation (Φ_{PA}). (*D*) Quantum efficiency of inactivation (Φ_{PI}). Data were fit to Eq. 1 for parameter estimation. Error bars represent SD with n ≧ 3.

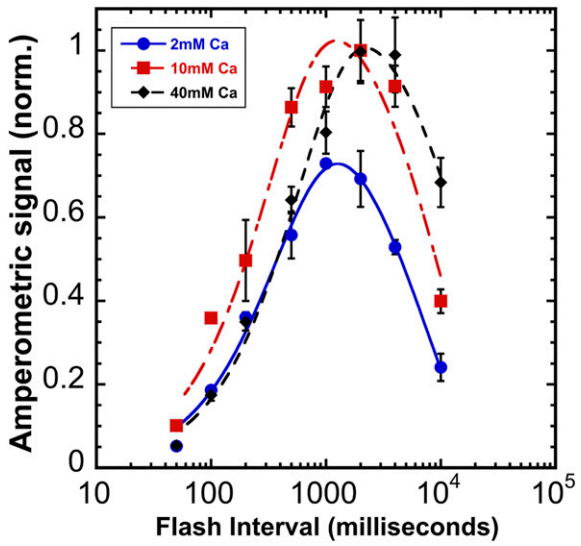

Fig. 3. Photoactivation yields as a function of flash interval at different calcium concentrations. Sequences of 150 Xe flashes applied at different flash intervals to HA-extracted thylakoid membranes from WT control and oxygen yields measured on a bare platinum electrode. Plots correspond to samples containing 2 (blue circle), 10 (red square), and 40 (black diamond) mM of $CaCl_2$ a fixed $[Mn^{2+}] = 250$ μM. Error bars represent SD with n ≧ 3. Data were fit to Eq. 2 to estimate the dark rearrangement constant, k_A, and the decay of photoactivation intermediates "B and C," k_D (see Fig. 1 for kinetic model and Table 1 for estimated values for k_A and k_D).

term, Φ_{PI}, represents the quantum efficiency of irreversible photodamage or, alternatively, the formation of inactive centers due to inappropriately bound Mn as a consequence of supraoptimal Mn^{2+} concentrations (22). This is also seen with varying $[Mn^{2+}]$ at fixed $[Ca^{2+}]$, where there is a strong dependence of Φ_{PI} on $[Mn^{2+}]$ (*SI Appendix*, Figs. S4 and S5). The corresponding estimates of parameters are plotted as a function of the Ca^{2+} concentration (Fig. 2 *C* and *D*). Additionally, the yields of photoactivation, indicated by the levels reached after ~500 flashes (Fig. 2 *A* and *B*), increase with $[Ca^{2+}]$ up to 10 mM Ca^{2+} at 250 μM Mn^{2+} and 20 mM Ca^{2+} at 500 μM Mn^{2+}, but higher $[Ca^{2+}]$ decreased yields, especially at 250 μM Mn^{2+}. Interestingly, at 250 μM Mn^{2+} the quantum efficiency of photoactivation, Φ_{PA}, is relatively unaffected by Ca^{2+} concentration throughout the range tested (Fig. 2*C*). In contrast, at the higher (500 μM Mn^{2+}) concentrations, Φ_{PA} is strongly dependent on Ca^{2+} availability, perhaps reflecting competitive occupation of Mn^{2+} in the Ca^{2+} effector site. As shown in Fig. 2*C*, at low $[Ca^{2+}]$, the Φ_{PA} is low, reaches a maximum at 20 mM coinciding with overall apparent optimum (Fig. 2*B*), and declines at higher $[Ca^{2+}]$. Overall, higher abundance of Mn^{2+} ions inhibits the assembly through competition with Ca^{2+} (11–13).

The difference between Φ_{PA} being unaffected by Ca^{2+} at 250 μM Mn^{2+} versus its being affected at 500 μM in Fig. 2*C* is intriguing and suggests a complex interplay of binding constants. The HAS likely remains occupied by Mn^{2+} (K_D < 10 μM) (13, 14, 16), with both the 250- and 500-μM Mn^{2+} experiments, even with comparatively high $[Ca^{2+}]$. However, at the higher $[Mn^{2+}]$ the results indicate that the Ca^{2+} effector site is substantially occupied by Mn^{2+}, leading to inactivation, consistent with previous kinetic analysis (12). It is unclear at which step(s) the replacing of Ca^{2+} ion with Mn ion is inhibitory; however, we find that Ca^{2+} can even be replaced with Mn in assembled PSII, producing a light-dependent inactivation during the catalytic turnover of the S-state cycle of the intact Mn cluster (*SI Appendix*, Fig. S6). This fits with the observation that Ca^{2+} is more readily released in the higher S-states, presumably due to charge repulsion (29, 30). Accordingly, the replacement of Ca^{2+} by Mn^{2+} at the Ca^{2+} site results not only in a failure to advance in photoassembly, but also a greater frequency of inactivation (Fig. 2*D*). The optimal Ca^{2+}/Mn^{2+} ratio for overall photoactivation thus reflects a balance between binding of Ca^{2+} at its effector site, which prevents photoinactivation due to inappropriate binding of Mn^{2+} (22), but not so high as to outcompete Mn^{2+} at a Mn site preventing photooxidative Mn incorporation (12–14). But which Mn site? Based upon the fact that Φ_{PA} at lower $[Mn^{2+}]$ is independent of $[Ca^{2+}]$ in the range tested, as well as previous estimates of Mn^{2+} affinity at the HAS, we conclude that the yield-limiting competition between Ca^{2+} at a Mn^{2+} site occurs not at the HAS, but rather at a second Mn site (SMS) involved in the photoactivation pathway. This is consistent with the results of the effect of $[Ca^{2+}]$ on the rate of the dark rearrangement step, k_A (next section).

Calcium Stabilizes Intermediates of Photoactivation and Prolongs the Dark Rearrangement Time. To test the hypothesis that Ca^{2+} influences the stability of the assembly intermediates, photoactivation was performed varying $[Ca^{2+}]$ and the time interval between photoactivating xenon light flashes (Fig. 3). According to the two-quantum model of photoactivation (Fig. 1) the initial photooxidation of Mn^{2+} (state "A") produces the first unstable intermediate "B," followed by a light-independent "rearrangement" step, leading to the formation of a second unstable intermediate "C," which is a configuration capable of productively utilizing the second light quantum to form the first stable intermediate, "D" (8). Short intervals produce low yields since not enough time has elapsed for completion of the dark rearrangement. Long intervals between the charge separations allow the decay of intermediates resulting in low yields of active centers (8, 9). This results in a bell-shaped curve recording the yield of photoactivation due to a fixed number of flashes given at different flash intervals from 50 to 10,000 ms (Fig. 3). Estimations of the parameters under each condition (Table 1) describing the dark rearrangement, k_A, and the decay of intermediates, k_D, were determined by deriving kinetic parameters from the rising and falling slopes of the bell-shaped curve in plots of photoactivation as a function of the flash interval curve fitted to Eq. 2:

$$[A]_n = [k_A/k_D - k_A] \times [A]_O \times (e^{-k_A td} - e^{-k_D td}) \qquad [2]$$

The overall shape of the resultant bell-shaped curves closely resembles previous results using higher plant material with estimated values for dark rearrangement (k_A, B➡C), and the decay of intermediates (k_D, B and C) are in the range of 200–400 ms and 7–14 s, respectively, in our experiments

Table 1. Dark rearrangement, k_A, and decay of intermediates, k_D, parameters characteristic of photoactivation of membranes from WT, ΔpsbO, and 27OE strains

Strain/$[Ca^{2+}]$ (mM Ca^{2+})	k_A (s^{-1}) ($t_{1/2}$ [ms])	k_D (s^{-1}) ($t_{1/2}$ [s])	Fit quality, *r*
WT control, 2	2.4 (288)	0.134 (5.17)	0.99
WT control, 10 mM Ca^{2+}	2.8 (244)	0.095 (7.29)	0.98
WT control, 40 mM Ca^{2+}	1.6 (433)	0.051 (13.5)	0.99
ΔpsbO, 2 mM Ca^{2+}	1.9 (364)	0.104 (6.66)	0.99
ΔpsbO, 10 mM Ca^{2+}	2.2 (315)	0.072 (9.62)	0.99
ΔpsbO, 40 mM Ca^{2+}	1.5 (462)	0.049 (14.1)	0.99
27OE, 2 mM Ca^{2+}	1.5 (462)	0.130 (5.33)	0.98
27OE, 10 mM Ca^{2+}	1.4 (495)	0.085 (8.15)	0.99
27OE, 40 mM Ca^{2+}	1.8 (385)	0.027 (25.6)	0.99

Data were fit to Eq. 2 to estimate the dark rearrangement constant, k_A, and the decay of photoactivation intermediates "B and C," k_D (see Fig. 1 for model). Error bars represent standard deviation n ≧ 3.

(Table 1). These values are slower than with spinach PSII preparations, but in the same proportions with the dark rearrangement, k_A, typically 10-fold faster than the rate of decay, k_D (reviewed in ref. 18). These differences may be attributed to the different source of experimental material and/or choice of buffers (e.g., the sucrose concentration is much higher than typically used). Depending upon the [Ca^{2+}], different optima for maximal yields of photoactivation were observed with increasing Ca^{2+} giving increasingly longer optima for the length of the dark period between flashes (Fig. 3). Photoactivation with 40 mM Ca^{2+} enhanced yields at the longest interval tested (10 s), again suggesting that Ca^{2+} stabilizes the intermediates of photoactivation. Accordingly, the fit values for the decay of intermediates k_D, are shifted to slower rates of decay (Table 1). The stabilizing effect of Ca^{2+} on photoactivation intermediates contrasts with the existence of the optimal [Ca^{2+}]/[Mn^{2+}] (Fig. 2) ratio for the net yield under repetitive flashing at a constant interval (500 ms). The flash interval experiment also provides estimates for the second parameter in the two-quantum model, the dark rearrangement, k_A, (B➡C, Fig. 1). This is the time needed between flashes before subsequent flashes become productive, which is experimentally reflected by diminished yields of photoactivation at short flash intervals (Fig. 3). Remarkably, the rearrangement takes longer time to complete at high [Ca^{2+}] concentrations (Table 1).

Our analyses of the preceding results leads us to conclude that at high [Ca^{2+}], assembly occurs, albeit suboptimally, due to competition between metals for their respective sites as shown before (11–13). However, we now find that high [Ca^{2+}] also allows assembly at long flash intervals due to stabilization of intermediates "B" and/or "C" (Fig. 1). On the other hand, at low [Ca^{2+}], photoactivation yields are also decreased (Fig. 3), at least partly due to photoinactivation when incorrectly Mn^{2+} occupies the Ca^{2+} site. The protective function of Ca^{2+} is important also in PSII centers that already have been assembled (*SI Appendix*, Fig. S6) consistent with the proposed "gate-keeper" function observed with intact PSII preparations (28, 39). Thus, we conclude that Ca^{2+} is important for assembly because it stabilizes intermediate "B" and/or "C" and that it prevents inactivation and failure to advance due to inappropriate binding of Mn^{2+} into the Ca^{2+} site during assembly (12, 22). Besides its gate-keeping role, Ca^{2+} can also block the necessary binding of the second Mn^{2+} especially at very high [Ca^{2+}]/[Mn^{2+}] ratios. This accounts for the slowing of the very slow dark rearrangement (B➡C). While sufficient concentrations of Ca^{2+} increase the chance of successful formation of intermediate "C," an excess of Ca^{2+} competes with the binding of the second Mn^{2+} at the SMS, thereby delaying the time before the second Mn^{2+} ion can occupy its site for photooxidation. This competitive inhibition extends the time before the rearranged state can be trapped (C⇒D) until the competing Ca^{2+} is replaced with Mn^{2+} enabling the photooxidative formation of stable intermediate "D." This, in turn, suggests that the dark rearrangement consists of a molecular reorganization (e.g., conformational change) that is only fruitful if a second Mn^{2+} bound at its correct site.

Role of PsbO and Psb27 during Photoactivation. The PSII assembly cofactor protein, Psb27, which appears to facilitate diffusional access to the WOC assembly site (32, 33, 37), does so by interacting with the E-loop of CP43 to allosterically modify its conformation (36, 40), which is hinged (18) in a way that opens the WOC for greater diffusion into the sites of cofactor binding (33). Since the natural steady-state abundance of Psb27 in the cell likely evolved to cope with assembly and repair of only a fraction of centers from the total population of PSII in the cell, then there may not be enough copies of Psb27 to stoichiometrically service all PSII centers upon quantitative removal of the Mn cluster experimentally produced by HA extraction. Similarly, diffusion of Mn^{2+} and Ca^{2+} ion could also be limited by the presence of the extrinsic proteins, impeding photoassembly as previously suggested from in vivo experiments with mutants (33, 41). To address these considerations, the photoactivation of two *Synechocystis* mutants, *ΔpsbO* lacking PsbO (42), and a strain overexpressing Psb27 (*27OE*) (*SI Appendix*, Fig. S7), were investigated. Importantly, the more open configurations of the WOC in both strains enabled a net recovery of O_2 evolution under continuous illumination that was more than 50% higher than in the wild-type (WT) control (*SI Appendix*, Table S1). Additionally, the optimal [Ca^{2+}]/[Mn^{2+}] ratio for both mutants appears to be about twice as high compared to the WT control (80/1 vs. 40/1) indicating alterations of the donor side polypeptide structure have a differential effect with the demand for Ca^{2+} being higher and/or a lower than the demand for Mn^{2+} (Fig. 4). Interestingly, both mutants showed somewhat lower quantum efficiency, Φ_{PA}, compared to WT control; however, at higher [Ca^{2+}], the yield continued increasing without saturation or decline through the entire flash sequence, suggesting that while the demand for Ca^{2+} was higher, fewer centers were lost to photoinactivation (compare with WT in Fig. 2). Accordingly, *ΔpsbO* and *27OE* appeared less prone to photoinactivation (Φ_{PI}) compared to the WT control (Fig. 4 and *SI Appendix*, Figs. S8–S11) suggesting the open configuration diminishes the tendency for Mn^{2+} to occupy the Ca^{2+} effector site, but with the optimum [Ca^{2+}] shifted higher. These observations are consistent with increased diffusion of the metal cofactors inside apo-PSII with proportionally increased exchange rates for Ca^{2+} at its effector site. Neither mutant showed a strong correlation between [Ca^{2+}] and quantum efficiency of photoactivation (Fig. 4*C*), which is similar to WT control preparations at the lower, 250 μM [Mn^{2+}] tested, but not the higher, 500 μM [Mn^{2+}]. Photoinactivation rate (Fig. 4*D*) is negligible for both mutant strains. With increased diffusional access, Ca^{2+} appears to more effectively prevent the inhibitory effect of Mn^{2+} on photoassembly. Notably, *ΔpsbO* and *27OE* show different Mn-dependent photoactivation behavior compared to WT control. While *27OE* has a requirement similar to the WT control for Mn^{2+} ions, with the optimum at 250 μM at 10 mM Ca^{2+}, *ΔpsbO* appears to have a lower requirement for available Mn^{2+} and shows maximal yield of photoactivation in the range of concentrations from 50 to 500 μM (*SI Appendix*, Figs. S8–S11).

As with the WT, the flash interval experiment shows that at longer intervals between flashes, Ca^{2+} stabilizes assembly intermediates (Fig. 5) as reflected in the slower decay constant, k_D (Table 1). However, *27OE* decreases in k_D overall, further slowing the decay with the increase of [Ca^{2+}], suggesting a possible role for Psb27 in stabilizing the photoactivation intermediates "B" and/or "C" (Fig. 1), perhaps by stabilizing the binding of Ca^{2+} at its effector site. Additionally, the dark rearrangement, k_A, is generally slower than the WT for both *ΔpsbO* and *27OE* (Table 1), although higher [Ca^{2+}] does not further slow the dark rearrangement in *27OE* as it does for WT and *ΔpsbO*. Apparently, both high [Ca^{2+}] and the more open configuration of apo-PSII leads to a slower dark rearrangement, k_A (Table 1), yet promotes better exchange of Ca^{2+} and prevents the decay of the photoactivation intermediates (Table 1). The increased stabilization of intermediates in *27OE* in comparison with *ΔpsbO* accords with the differences in the final yields of active centers as a function of flash number at different [Ca^{2+}] (Fig. 4*A* vs. Fig. 4*B*). Note, for example, that the 10 mM Ca^{2+} reaction in *27OE* produces higher yields compared to *ΔpsbO*, closely approaching the yields at the optimal 20 mM [Ca^{2+}]. Taken together, the results suggest that Psb27 enhances the stabilization of intermediates with accessibility of the site of cluster assembly, especially for Ca^{2+} ions, thereby shifting the optimal ratio of Mn^{2+} and Ca^{2+}. As discussed, given the known characteristics of the interaction of Psb27 with apo-PSII (36),

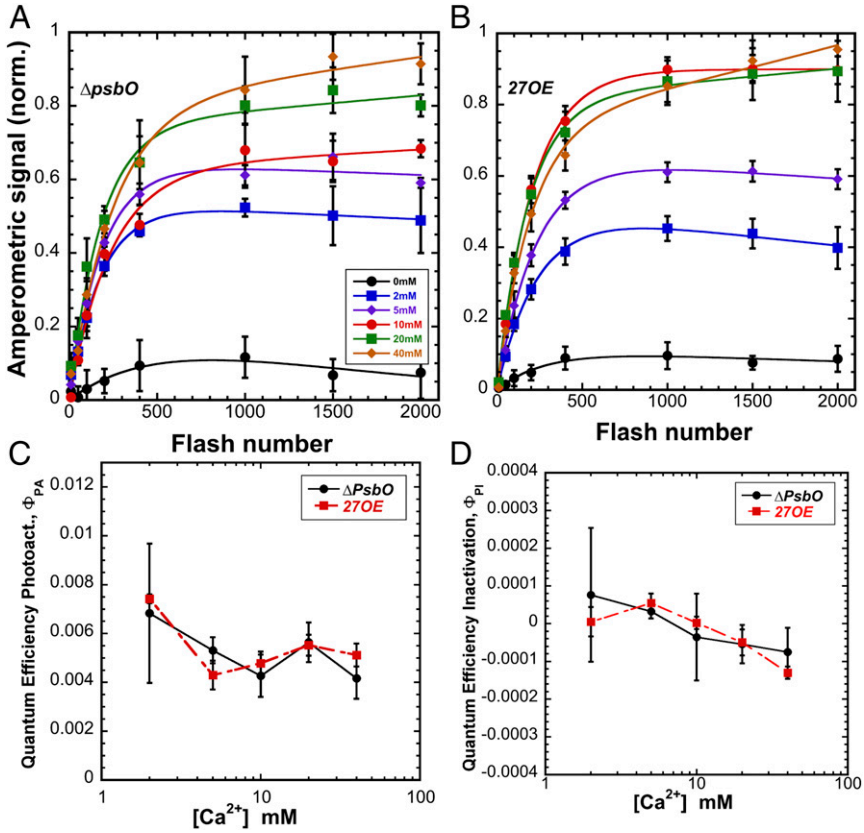

Fig. 4. Calcium dependence of photoactivation under sequence of single turnover flashes at 2 Hz (500-ms flash interval) of HA-extracted thylakoid membranes from *ΔpsbO* (*A*) and *27OE* (*B*) at 0 (black circle), 2 (blue square), 5 (purple diamond), 10 (red circle), 20 (green square), and 40 (orange diamond) mM of $CaCl_2$ combined with 250 μM $MnCl_2$. (*C*) Overall quantum efficiency of photoactivation (Φ_{PA}). (*D*) Quantum efficiency of inactivation (Φ_{PI}) in *ΔpsbO* (black circle) and *27OE* (red square) membranes, respectively. Data were fit to Eq. 1 for parameter estimation. Error bars represent SD with n ≧ 3.

this facilitation of photoactivation likely occurs allosterically via its interaction with the luminal E-loop of CP43, which, besides D1, provides a ligand to the mature Mn_4CaO_5.

Discussion

How Ca^{2+} Stabilizes Photoactivation Intermediates yet Retards the Dark Rearrangement. Our results show that Ca^{2+} stabilizes the assembly intermediates of photoactivation, a feature especially evident at long intervals between photoactivating flashes (Figs. 3 and 5). Moreover, the results also show that excess Ca^{2+} slows down the already very slow dark rearrangement (B➡C), an effect that is enhanced by the more open configuration of the apo-PSII assembly site in the mutants where greater ion exchange occurs (Figs. 3 and 5 and Table 1). According to the two-quantum model of photoactivation (8), a stable intermediate "D" is formed by two light-dependent steps separated by a light-independent rearrangement (Fig. 1). The first light-activated step (A⇒B) involves photooxidation of a single Mn^{2+} ion (8, 10, 12, 14) bound as hydroxide [(Mn)-OH^+] (15) at the HAS and occurs with high quantum efficiency (14, 16, 43, 44). The concurrent binding of Ca^{2+} at its adjacent effector site does not affect the affinity of the binding of this Mn^{2+}, but upon photooxidation of Mn^{2+} in the presence of bound Ca^{2+}, the bridging species, [Mn^{3+}-(OH^-)-Ca^{2+}] ⇌ [Mn^{3+}-(O^{2-})-Ca^{2+}], is produced (23), which is thought to facilitate the next steps. This rapid initial photooxidation (A⇒B) is followed by a remarkably slow (100–400 ms) rearrangement (B➡C), that involves a protein conformational change and/or ion relocation. Only then can the second charge separation become effective (C⇒D), photooxidizing a second Mn^{2+}, and thereby trapping the first stable intermediate "D" (8). Current models suggest this first stable intermediate, "D," is a binuclear (Mn^{3+})$_2$-(di-μ-oxo) bridged structure (9, 45), possibly corresponding to the binuclear di-μ-oxo bridged structure produced by partial disassembly of the intact Mn_4CaO_5 using reducing agents (26, 28) or thermal (45) treatment.

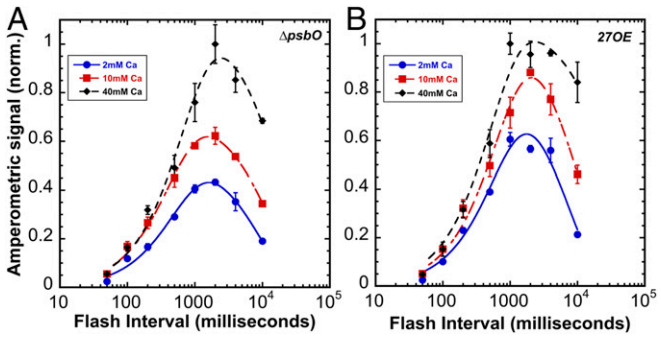

Fig. 5. Photoactivation yields as a function of flash interval at different calcium concentrations. Sequences of 150 Xe flashes applied at different flash intervals to HA-extracted thylakoid membranes from *ΔpsbO* (*A*) and *27OE* (*B*) with O_2 yields measured on a bare platinum electrode. Plots correspond to samples containing 2 (blue circle), 10 (red square), and 40 (black diamond) mM of $CaCl_2$ at a fixed [Mn^{2+}] = 250 μM. Error bars represent SD with n ≧ 3. Data were fit to Eq. 2 to estimate the dark rearrangement constant, k_A, and the decay of photoactivation intermediates "B and C," k_D (see Fig. 1 for kinetic model and Table 1 for estimated values for k_A and k_D).

Based upon the findings that Φ_{PA} at lower [Mn^{2+}] is independent of [Ca^{2+}] (Fig. 2*C*) combined with estimates of Mn^{2+} affinity at the HAS (K_D < 10 μM) (13, 14, 16), we infer that the competition between Ca^{2+} for a critical Mn^{2+} site occurs not at the HAS, but rather at an SMS involved in the photoactivation pathway and that excess Ca^{2+}, while protecting from photoinactivation, inhibits assembly due to occupation of the SMS preventing photooxidation of the second Mn^{2+} (C⇒D). The present experiments cannot discriminate the identity of the SMS, although it is reasonable to suppose the SMS includes ligands that form with the other Mn1-Mn3 positions (*SI Appendix*, Fig. S1*B*, orange spheres), and that corresponds to the site estimated to have K_D~50 μM from steady-state photoactivation experiments (12). It also does not exclude the possibility, for example, that the Mn^{3+} ion initially produced from Mn^{2+} at the HAS (A⇒B) relocates to the SMS as part of the dark rearrangement (B➞C), according to the "translocation model" (7, 46).

The stabilization of intermediates (B, C) by Ca^{2+} is most simply explained in the same way that Ca^{2+} prevents the photoinactivation of apo-PSII. Photoinactivation is due to incorrect occupation of the Ca^{2+} effector site (CAS) by Mn^{2+} evident at suboptimal Ca^{2+}/Mn^{2+} ratios, which can even occur in intact PSII (*SI Appendix*, Fig. S6) in line with the proposed gate-keeper function of Ca^{2+} in the assembled Mn_4CaO_5 (26, 28, 39). Furthermore, Ca^{2+} tends to be lost from its effector site due to the electrostatic repulsion occurring upon oxidation of Y_Z (30) and/or associated pK_a changes (29). Although the mechanism of Mn-dependent inactivation is not clear, occupation of the CAS by Mn^{2+} correlates with photoinactivation, as well as "misses" due to the requirement for Ca^{2+} to form the necessary bridging species with Mn at the HAS needed for advancement through the assembly sequence (23). Accordingly, the occupation of the CAS by Ca^{2+} is important throughout the duration of the dark rearrangement (B➞C). The observation that both *ΔpsbO* and *27OE* each exhibit minimal photoinactivation suggests that ion exchange at the Ca^{2+} site is rapid in the more open configuration, and this enables centers that have lost the Ca^{2+} ion to rapidly reacquire a replacement.

Besides stabilizing intermediates, Ca^{2+} also slows the dark rearrangement (Figs. 3 and 5 and Table 1). At supraoptimal concentrations, Ca^{2+} appears to block the necessary binding of the second Mn^{2+}, at the second Mn-binding site, SMS, as already noted. While sufficient concentrations of Ca^{2+} increase the chance of successful formation of intermediate "C," an excess of Ca^{2+} competes with the binding of the second Mn^{2+}-binding site, thereby delaying the time before the second Mn^{2+} ion can occupy the SMS for photooxidation, forming the first stable intermediate "D," which is predicted to be a binuclear $(Mn^{3+})_2$-(di-μ-oxo) bridged structure (9, 45). However, if Ca^{2+} competitively occupies the second Mn^{2+} site, then the rearranged configuration cannot be productively converted due to the absence of the second Mn^{2+} needed for the photooxidative second light step (C⇒D). This proposed model suggests that the dark rearrangement consists of a molecular reorganization (e.g., conformational change and/or ion relocation) that is only ready for photooxidative stabilization (C⇒D), if a second Mn^{2+} bound at its correct site, the SMS.

How Does Psb27 Facilitate Photoactivation? It has been shown that Psb27 is the vital player in PSII repair and assembly of the Mn_4CaO_5 cluster of PSII that provides greater accessibility to the site of Mn-cluster assembly (32, 33, 36, 47–49). We find that Psb27 facilitates the photoactivation of the WOC in a more complex manner than simply displacing extrinsic polypeptides from apo-PSII. Both *ΔpsbO* and *27OE* have increased access of Mn^{2+} and Ca^{2+} to the apo-PSII consistent with expectations (reviewed in ref. 25), and also both mutations produce shifts toward higher optimal [Ca^{2+}]/[Mn^{2+}] ratios. In the absence of extrinsic proteins, light induces the loss of Ca^{2+} from its binding site in an S-state dependent manner (29, 30), and one of the main functions of the extrinsic proteins is to retain the ion (50, 51). Thus, the shift to higher optimal [Ca^{2+}]/[Mn^{2+}] ratios in the mutants is likely because in the absence of retention of Ca^{2+} in the vicinity of the assembly site, a relatively higher [Ca^{2+}] is required. However, if the function of Psb27 only increased exchangeability of Ca^{2+}, then *ΔpsbO* and *27OE* would have similar phenotypes in regard to photoactivation. This was not the case, and *27OE* provides additional support of photoactivation: *27OE* exhibits a remarkable stabilization at high [Ca^{2+}], yet does not exhibit a proportionally dramatic increase in the dark rearrangement time at the highest [Ca^{2+}] as seen with *ΔpsbO* (Table 1). Additionally, it has a greater ability to sustain high yields of photoactivation at moderate [Ca^{2+}] compared to *ΔpsbO* (Fig. 4). Chemical crosslinking indicates that Psb27 docks to the outer face (distal to the Mn-assembly site) of the E-loop of CP43 and exerts its effects, including the weakened binding of extrinsic proteins, allosterically (36), and the strength of this interaction changes during the proteolytic processing of the C terminus of the D1 protein (40). This suggests that the Psb27–E-loop interaction stabilizes a structural arrangement that 1) enhances the selectivity of the second Mn^{2+} photooxidation site *vis-á-vis* the competitive binding of Ca^{2+} at the SMS, 2) stabilizes the binding of Ca^{2+} to the CAS, and 3) maintains an open configuration that enables rapid rebinding of Ca^{2+} if the ion is lost from the Ca-effector site and/or facilitates the exchange of metals in malformed metal centers.

What Is the Dark Rearrangement? The utilization of single turnover flashes during the flash interval experiment ensures that the dark rearrangement (B➞C) estimates the rate, k_A, of a molecular process proposed to be a conformational change (22, 38, 41, 52) or the relocation of a bound ion (7, 46). Once the rearrangement has occurred, the still labile configuration can be stabilized by a second quantum causing the photooxidation of the second Mn^{2+} at the SMS, to produce the first stable intermediate, "D" (Fig. 1). Based upon the observation that Psb27 allosterically modulates the assembly of the Mn_4CaO_5, we suppose that the mobility of the E-loop is part of the dark rearrangement process. The E-loop is a globular domain situated between transmembrane helices 5 and 6 of CP43 and directly interacts with the assembled Mn_4CaO_5, including a bridging carboxylate ligand to Mn2 and Mn3 via CP43-Glu354 (5). Moreover, it directly contacts the C-terminal domain of the D1-protein, which contains amino acids coordinating the Mn_4CaO_5 and notably provides a ligand to the Ca^{2+} and Mn1 via the carboxyl group of its C terminus. Thus, movements of the E-loop during photoactivation are likely coupled to movements of the C-terminal domain, and vice versa (18). A recent cryo-EM structure resolution of apo-PSII shows alternative structural arrangements of the apo-WOC, including the E-loop displaced away from the HAS, which is itself rearranged compared the coordination environment of the assembled Mn_4CaO_5 (53), and a recent time-resolved AFM study has demonstrated that the E-loop undergoes hinged stochastic fluctuations (54). The increased accessibility in *ΔpsbO* cannot be explained by steric covering of the apo-WOC, and instead, the open configuration must relate to the fact that PsbO forms a structural bridge between the E-loop and other parts of the WOC including the D1 C-terminal domain (*SI Appendix*, Fig. S1*A*). Thus, the more open configuration due to the loss of PsbO is likely due to enhanced mobility of the WOC. The position of the E-loop may be stabilized by Psb27, so that it still may fluctuate, but in a range that optimizes assembly, in contrast to the loss of PsbO, where the more open configuration is evident, but not the other kinetic features, which are absent. However, the predicted mobility of the apo-WOC alone does not explain the conformational rearrangement because the rate, k_A, slows down

rather than speeds up in the mutants, and it is strongly affected by [Ca^{2+}]. So, while conformational mobility of the E-loop and the associated D1-carboxyl terminus is a reasonable explanation for the more open structure, how excess Ca^{2+} would also slow the rearrangement process is not obvious. This is where the SMS may factor in: if the dark rearrangement corresponds to conformational fluctuations alternating between the open and closed configurations, then a specific closed conformation may be necessary for Mn^{2+} ligation and/or photooxidation at the SMS. Indeed, the actual formation SMS ligation environment may be contingent upon the rearrangement. Furthermore, if the specific closed conformation is only infrequently realized during the course of conformational fluctuations, as suggested by the dwell times of the open and closed conformations (54), then competitive occupation of the SMS by Ca^{2+} would delay the time until Mn^{2+} reoccupies the SMS and the specific conformation is revisited during the course of the conformational fluctuations. In this model, the rearrangement rate reflects the frequency of occurrence that intermediate, "B"-containing Mn^{3+} has conformationally rearranged, the intrinsic protein conformational rearrangement time, and the SMS site is actually occupied by a Mn^{2+} ion (Fig. 6).

In conclusion, the initial stages of photoactivation appear to involve three critical metal-binding sites: two Mn (HAS, SMS) and one Ca (CAS). These sites are utilized for photooxidative metal cluster formation in a process that involves structural rearrangements of the protein scaffolding that templates the assembly. Occupation of the CAS by Ca^{2+} is critical for stabilizing assembly intermediates during the dark rearrangement (B➡C). Incorrect occupation of the CAS by Mn^{2+}, e.g., at suboptimal Ca/Mn ratios, results in photochemical misses and a photoinactivation process that probably corresponds to the Mn^{2+} photooxidation pathway leading of high-valence, but misassembled Mn (22). The long-observed competition between Mn^{2+} and Ca^{2+} appears to occur at the SMS, and the occupation of this site by competing Ca^{2+} ions slows the dark rearrangement. The results are most easily rationalized in a model where the dark rearrangement involves the conformational mobility of the WOC domain, which fluctuates in the absence of the Mn_4CaO_5 (54) (Fig. 6). In this model, the trapping of the first stable state "D" occurs when three conditions are met simultaneously: 1) the rearranging WOC assumes an optimal structural geometry, 2) the metal-binding sites are appropriately occupied, and 3) photochemistry generates an oxidant to oxidize the second Mn^{2+} (C⇒D). According to this model, the accessory protein Psb27 allosterically constrains structural fluctuations in the apo-WOC in a way that optimizes the assembly by stabilizing the intermediates and the promoting productive occupancy of the metal-binding sites by their cognate ions.

Materials and Methods

Strains and Growth Conditions. The glucose-tolerant *Synechocystis* sp. PCC6803 control strain (WT control) expressing only the WT *psbA2* gene and having a hexa-histidine tag fused to the carboxyl-terminus of CP47 was maintained in BG-11 medium, as described previously (55). Experimental cultures were grown in flat 1L tissue culture flasks in 800 mL BG-11 media buffered with 10 mM Hepes-NaOH pH 8.0 (HBG-11) supplemented with 5 mM glucose (Sigma) under a PFD (photon flux density) of ~80 μmol m^{-2} s^{-1} at 30 °C. Cultures were bubbled with filter-sterilized air. Light intensity measurements were made with a Walz light meter (Germany).

Mutant Strain Generation. The *ΔpsbO* deletion mutant was constructed previously and involved replacement of the *psbO* coding sequence with an Sp^r/Sm^r antibiotic resistance gene (42). For overexpression of Psb27 gene in *Synechocystis*, the chromosomal locus comprising the ORF slr1645 (Psb27) was amplified by PCR (*SI Appendix*, Table S2) using Herculase II Phusion DNA polymerase (Agilent) and integrated at a neutral site within the *Synechocystis* genome between ORFs slr1169 and slr1285 (*SI Appendix*, Fig. S12). Transformation was carried as described previously using selective agar plates containing 5 mM glucose, 10 μM DCMU, and 12.5 μg/mL spectinomycin followed by further selection at 25 μg/mL spectinomycin (56).

Preparation of Mn-Depleted Thylakoid Membranes. Cultures (2.4 L) were harvested in early stationary phase (OD_{750nm} ~1.8–2.2) and exhibited variable Chl fluorescence ($[F_m - F_0]/F_0$) values >0.5, as measured with a Photon Systems Instruments (PSI) Fluorometer FL 3500. Cells were collected by centrifugation at 25 °C at 6,000 *g* (Sorvall, F-9 rotor) for 15 min and gently resuspended with a minimal volume of H20BG-11(same as growth media, but with 20 mM Hepes-NaOH pH 8.0) using a paintbrush. The cell suspension

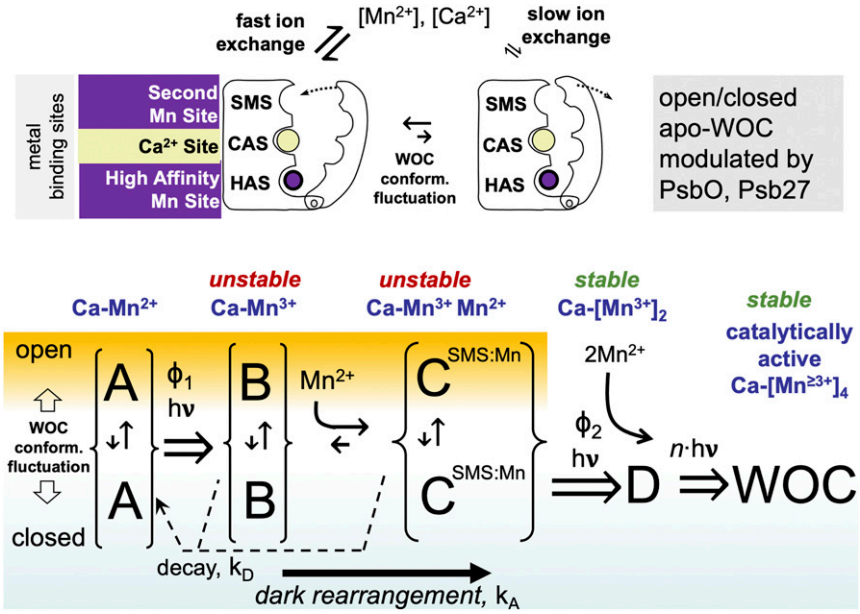

Fig. 6. Schematic model of the three main metal-binding sites discussed and a minimal model of photoactivation with proposed conformational change and ion exchange accounting for the results. Brackets around individual states A, B, and C indicate alternate protein conformations with similar bound ion states (blue text in figure). Dark decay (k_D) of states B and C to A indicated with arrows with dotted lines. Dark rearrangement (B➡C, solid arrow below) is proposed to include ion binding and conformational changes of the CP43 e-loop and D1-carboxyterminal domain. Only the productive pathway involving binding of Mn^{2+} to the SMS indicated by $C^{SMS:Mn}$ during dark rearrangement is shown, but the not the nonproductive Ca^{2+} binding at the SMS (*SI Appendix*, Fig. S1).

volume was expanded to ~200 mL with additional H20BG-11. The washed cells were centrifuged again at 25 °C at 10,200 *g* for 5 min (Sorvall, F-14 rotor). The pelleted cells were resuspended as before in H20BG-11 medium, and the suspension was adjusted to a Chl concentration of 100 μg mL^{-1} Chl. Hydroxylamine was added to 1 mM from a freshly prepared 400 mM stock, and the treated suspension was incubated for 12 min in the darkness with rotary agitation (200 rpm) at room temperature. Maintaining complete darkness, the HA-extracted cells were then washed by resuspension with 100 mL H20BG-11 and rotary agitation (200 rpm) for 5 min before pelleting again. This washing step was repeated four more times with the aim of depleting residual HA. Finally, the cells were resuspended in 120 mL of breaking buffer (1.2 M betaine, 50 mM MES-NaOH [pH 6.0], 10% [vol/vol] glycerol, and 5 mM $MgCl_2$) that was prepared with ultrapure reagents and Chelex-100 (Bio-Rad)–treated solutions and incubated in the dark on ice for 1 h. Cells were pelleted at 10,200 *g* for 5 min and resuspended to a total volume of 14 mL. Prior to cell breakage, 1 mM benzamidine, 1 mM ε-amino–n-caproic acid, 1 mM phenylmethylsulfonyl fluoride, and 0.05 mg/mL DNase I were added. Cells were broken by four cycles of 5 s ON and 5 min OFF in an ice-cooled glass bead homogenizer (Bead-Beater, BioSpecProducts, USA). After breakage the sample was centrifuged at 3,600 *g* for 10 min to pellet unbroken cells and cell debris. Thylakoids were obtained from the supernatant cell homogenate by ultracentrifugation (35 min at 40,000 rpm in a Beckman Ti45 rotor), and thylakoid-containing pellets were suspended in Chelex-100–treated breaking buffer to a concentration of 1.0–1.5 mg of Chl mL^{-1}. Concentrated thylakoid membranes were flash-frozen as 100 μL aliquots in liquid nitrogen and stored at −80 °C.

Photoactivation of HA-Extracted Membranes. HA-extracted membranes were photoactivated either in suspension for subsequent assay for restoration of O_2 evolution detected using a Clark-type electrode or directly on a bare platinum electrode that permits the centrifugal deposition of samples upon the electrode surface (16). Flash illumination under each mode of photoactivation was provided using an EG&G xenon flash lamp. The buffer was supplemented with various concentrations of cations $CaCl_2$, $MnCl_2$, $SrCl_2$, and $MgCl_2$ to examine their role in photoactivation for the role of cations on photoactivation. See *SI Appendix, Supplementary Materials* for details for data collection and data processing.

Data Availability. All study data are included in the article and supporting information.

ACKNOWLEDGMENTS. The authors wish to thank Prof. Charles Yocum for stimulating discussions and great technical advice. R.L.B. gratefully acknowledges support from the Vaughn O. Vennerberg III fund. This work was funded by the NSF (MCB-1716408).

1. D. J. Vinyard, G. W. Brudvig, Progress toward a molecular mechanism of water oxidation in photosystem II. *Annu. Rev. Phys. Chem.* **68**, 101–116 (2017).
2. W. Lubitz, M. Chrysina, N. Cox, Water oxidation in photosystem II. *Photosynth. Res.* **142**, 105–125 (2019).
3. H. Dau, E. Fujita, L. Sun, Artificial photosynthesis: Beyond mimicking nature. *ChemSusChem* **10**, 4228–4235 (2017).
4. D. A. Lutterman, Y. Surendranath, D. G. Nocera, A self-healing oxygen-evolving catalyst. *J. Am. Chem. Soc.* **131**, 3838–3839 (2009).
5. Y. Umena, K. Kawakami, J. R. Shen, N. Kamiya, Crystal structure of oxygen-evolving photosystem II at a resolution of 1.9 Å. *Nature* **473**, 55–60 (2011).
6. T. Cardona, A. Sedoud, N. Cox, A. W. Rutherford, Charge separation in photosystem II: A comparative and evolutionary overview. *Biochim. Biophys. Acta* **1817**, 26–43 (2012).
7. H. Bao, R. L. Burnap, Photoactivation: The light-driven assembly of the water oxidation complex of photosystem II. *Front. Plant Sci.* **7**, 578 (2016).
8. R. Radmer, G. M. Cheniae, Photoactivation of the manganese catalyst of 0 2 evolution II. A two-guantum mechanism. *Biochim. Biophys. Acta* **253**, 182–186 (1971).
9. N. Tamura, G. Cheniae, Photoactivation of the water-oxidizing complex in photosystem II membranes depleted of Mn and extrinsic proteins. I. Biochemical and kinetic characterization. *Biochim. Biophys. Acta* **890**, 179–194 (1987).
10. G. M. Cheniae, I. F. Martin, Photoactivation of the manganese catalyst of O_2 evolution. I. Biochemical and kinetic aspects. *Biochim. Biophys. Acta* **253**, 167–181 (1971).
11. T. A. Ono, Y. Inoue, Requirement of divalent cations for photoactivation of the latent water oxidation system in intact chloroplasts from flashed leaves. *Biochim. Biophys. Acta* **723**, 191–201 (1983).
12. A. F. Miller, G. W. Brudvig, Manganese and calcium requirements for reconstitution of oxygen-evolution activity in manganese-depleted photosystem II membranes. *Biochemistry* **28**, 8181–8190 (1989).
13. G. M. Ananyev, G. C. Dismukes, High-resolution kinetic studies of the reassembly of the tetra-manganese cluster of photosynthetic water oxidation: Proton equilibrium, cations, and electrostatics. *Biochemistry* **35**, 14608–14617 (1996).
14. T. A. Ono, H. Mino, Unique binding site for Mn^{2+} ion responsible for reducing an oxidized Y_Z tyrosine in manganese-depleted photosystem II membranes. *Biochemistry* **38**, 8778–8785 (1999).
15. G. M. Ananyev, A. Murphy, Y. Abe, G. C. Dismukes, Remarkable affinity and selectivity for Cs+ and uranyl (UO22+) binding to the manganese site of the apo-water oxidation complex of photosystem II. *Biochemistry* **38**, 7200–7209 (1999).
16. P. J. Nixon, B. A. Diner, Aspartate 170 of the photosystem II reaction center polypeptide D1 is involved in the assembly of the oxygen evolving manganese cluster. *Biochemistry* **31**, 942–948 (1992).
17. R. J. Boerner, A. P. Nguyen, B. A. Barry, R. J. Debus, Evidence from directed mutagenesis that aspartate 170 of the D1 polypeptide influences the assembly and/or stability of the manganese cluster in the photosynthetic water-splitting complex. *Biochemistry* **31**, 6660–6672 (1992).
18. R. L. Burnap, D1 protein processing and Mn cluster assembly in light of the emerging photosystem II structure. *Phys. Chem. Chem. Phys.* **6**, 4803–4809 (2004).
19. M. Miyao-Tokutomi, Y. Inoue, Improvement by benzoquinones of the quantum yield of photoactivation of photosynthetic oxygen evolution: Direct evidence for the two-quantum mechanism. *Biochemistry* **31**, 526–532 (1992).
20. M. Ibrahim *et al*., Untangling the sequence of events during the S(2) → S(3) transition in photosystem II and implications for the water oxidation mechanism. *Proc. Natl. Acad. Sci. U.S.A.* **117**, 12624–12635 (2020).
21. N. Tamura, Y. Inoue, G. Cheniae, Photoactivation of the water-oxidizing complex in photosystem II membranes depleted of Mn, Ca, and extrinsic proteins. II. Studies on the function of Ca^{2+}. *Biochim. Biophys. Acta* **976**, 173–181 (1989).
22. C. Chen, J. Kazimir, G. M. Cheniae, Calcium modulates the photoassembly of photosystem II (Mn)4 clusters by preventing ligation of nonfunctional high valency states of manganese. *Biochemistry* **34**, 13511–13526 (1995).
23. A. M. Tyryshkin *et al*., Spectroscopic evidence for Ca^{2+} involvement in the assembly of the Mn_4Ca cluster in the photosynthetic water-oxidizing complex. *Biochemistry* **45**, 12876–12889 (2006).
24. D. J. Vinyard *et al*., Photosystem II oxygen-evolving complex photoassembly displays an inverse H/D solvent isotope effect under chloride-limiting conditions. *Proc. Natl. Acad. Sci. U.S.A.* **116**, 18917–18922 (2019).
25. J. L. Roose, L. K. Frankel, M. P. Mummadisetti, T. M. Bricker, The extrinsic proteins of photosystem II: Update. *Planta* **243**, 889–908 (2016).
26. R. Mei, C. F. Yocum, Comparative properties of hydroquinone and hydroxylamine reduction of the Ca(2+)-stabilized O2-evolving complex of photosystem II: Reductant-dependent Mn2+ formation and activity inhibition. *Biochemistry* **31**, 8449–8454 (1992).
27. N. Tamura, G. Cheniae, Effects of photosystem II extrinsic proteins on microstructure of the oxygen-evolving complex and its reactivity to water analogs. *Biochim. Biophys. Acta* **809**, 245–259 (1985).
28. R. Mei, C. F. Yocum, Calcium retards NH2OH inhibition of O2 evolution activity by stabilization of Mn2+ binding to photosystem II. *Biochemistry* **30**, 7836–7842 (1991).
29. A. Boussac, A. W. Rutherford, Ca^{2+} binding to the oxygen evolving enzyme varies with the redox state of the Mn enzyme. *FEBS Lett.* **236**, 432–436 (1988).
30. M. Miqyass, M. A. Marosvölgyi, Z. Nagel, C. F. Yocum, H. J. van Gorkom, S-state dependence of the calcium requirement and binding characteristics in the oxygen-evolving complex of photosystem II. *Biochemistry* **47**, 7915–7924 (2008).
31. Y. Kashino *et al*., Proteomic analysis of a highly active photosystem II preparation from the cyanobacterium *Synechocystis* sp. PCC 6803 reveals the presence of novel polypeptides. *Biochemistry* **41**, 8004–8012 (2002).
32. M. M. Nowaczyk *et al*., Psb27, a cyanobacterial lipoprotein, is involved in the repair cycle of photosystem II. *Plant Cell* **18**, 3121–3131 (2006).
33. J. L. Roose, H. B. Pakrasi, The Psb27 protein facilitates manganese cluster assembly in photosystem II. *J. Biol. Chem.* **283**, 4044–4050 (2008).
34. H. Chen *et al*., A Psb27 homologue in *Arabidopsis thaliana* is required for efficient repair of photodamaged photosystem II. *Plant Mol. Biol.* **61**, 567–575 (2006).
35. F. Bentley, J. Eaton-Rye, Psb27 is required for photoinactivation and recovery of photosystem II in *Synechocystis* sp PCC6803 cells lacking PsbV. *Photosynth. Res.* **91**, 204 (2007).
36. H. Liu, R. Y. Huang, J. Chen, M. L. Gross, H. B. Pakrasi, Psb27, a transiently associated protein, binds to the chlorophyll binding protein CP43 in photosystem II assembly intermediates. *Proc. Natl. Acad. Sci. U.S.A.* **108**, 18536–18541 (2011).
37. J. Komenda *et al*., The Psb27 assembly factor binds to the CP43 complex of photosystem II in the cyanobacterium *Synechocystis* sp. PCC 6803. *Plant Physiol.* **158**, 476–486 (2012).
38. L. Zaltsman, G. M. Ananyev, E. Bruntrager, G. C. Dismukes, Quantitative kinetic model for photoassembly of the photosynthetic water oxidase from its inorganic constituents: Requirements for manganese and calcium in the kinetically resolved steps. *Biochemistry* **36**, 8914–8922 (1997).
39. J. Tso, M. Sivaraja, G. C. Dismukes, Calcium limits substrate accessibility or reactivity at the manganese cluster in photosynthetic water oxidation. *Biochemistry* **30**, 4734–4739 (1991).
40. H. Liu *et al*., Mass spectrometry-based footprinting reveals structural dynamics of loop E of the chlorophyll-binding protein CP43 during photosystem II assembly in the cyanobacterium *Synechocystis* 6803. *J. Biol. Chem.* **288**, 14212–14220 (2013).
41. R. L. Burnap, M. Qian, S. Al-Khaldi, C. Pierce, "Photoactivation and S-state cycling kinetics in photosystem II mutants in *Synechocystis* sp. PCC6803" in *Photosynthesis: From Light to Biosphere, P. Mathis, Ed.*, (Kluwer, Dordrecht, The Netherlands, 1995), pp. 443–446.
42. R. L. Burnap, L. A. Sherman, Deletion mutagenesis in *Synechocystis* sp. PCC6803 indicates that the Mn-stabilizing protein of photosystem II is not essential for O2 evolution. *Biochemistry* **30**, 440–446 (1991).

43. C. W. Hoganson, D. F. Ghanotakis, G. T. Babcock, C. F. Yocum, Manganese ion reduces redox activated tyrosine in manganese-depleted photosystem II preparations. *Photosynth. Res.* **22**, 285–294 (1989).
44. B. A. Diner, P. J. Nixon, The rate of reduction of oxidized redox-active tyrosine, Z^+, by exogenous Mn^{2+} is slowed in a site-directed mutant, at aspartate 170 of polypeptide D1 of photosystem II, inactive for photosynthetic oxygen evolution. *Biochim. Biophys. Acta* **1101**, 134–138 (1992).
45. M. Barra *et al*., Intermediates in assembly by photoactivation after thermally accelerated disassembly of the manganese complex of photosynthetic water oxidation. *Biochemistry* **45**, 14523–14532 (2006).
46. M. Zhang *et al*., Structural insights into the light-driven auto-assembly process of the water-oxidizing Mn_4CaO_5-cluster in photosystem II. *eLife* **6**, e26933 (2017).
47. J. L. Roose, H. B. Pakrasi, Evidence that D1 processing is required for manganese binding and extrinsic protein assembly into photosystem II. *J. Biol. Chem.* **279**, 45417–45422 (2004).
48. C. Xingxing *et al*., Crystal structure of Psb27 from *Arabidopsis thaliana* determined at a resolution of 1.85 Å. *Photosynth. Res.* **136**, 139–146 (2018).
49. F. Michoux *et al*., Crystal structure of the Psb27 assembly factor at 1.6 Å: implications for binding to Photosystem II. *Photosynth. Res.* **110**, 169–175 (2012).
50. J. P. Dekker, D. F. Ghanotakis, J. J. Plijter, G. H. J. Van, G. T. Babcock, Kinetics of the oxygen-evolving complex in salt-washed photosystem II preparations. *Biochim. Biophys. Acta* **767**, 515–523 (1984).
51. M. Miyao, N. Murata, Light-dependent inactivation of photosynthetic oxygen evolution during NaCl treatment of photosystem II particles: The role of the 24-kDa protein. *Photosynth. Res.* **10**, 489–496 (1986).
52. R. L. Burnap, M. Qian, C. Pierce, The manganese stabilizing protein of photosystem II modifies the in vivo deactivation and photoactivation kinetics of the H2O oxidation complex in *Synechocystis* sp. PCC6803. *Biochemistry* **35**, 874–882 (1996).
53. C. J. Gisriel *et al*., Cryo-EM structure of monomeric photosystem II from *Synechocystis* sp. PCC 6803 lacking the water-oxidation complex. *Joule* **4**, 2131–2148, 10.1016/j.joule.2020.07.016 (2020).
54. T. Tokano, Y. Kato, S. Sugiyama, T. Uchihashi, T. Noguchi, Structural dynamics of a protein domain relevant to the water-oxidizing complex in photosystem II as visualized by high-speed atomic force microscopy. *J. Phys. Chem. B* **124**, 5847–5857 (2020).
55. R. J. Debus *et al*., Does histidine 332 of the D1 polypeptide ligate the manganese cluster in photosystem II? An electron spin echo envelope modulation study. *Biochemistry* **40**, 3690–3699 (2001).
56. J. G. K. Williams, Construction of specific mutations in Photosystem II photosynthetic reaction center by genetic engineering methods in *Synechocystis* 6803. *Methods Enzymol.* **167**, 766–778 (1988).